Bioorganic Chemistry 88 (2019) 102963

Contents lists available at ScienceDirect

Bioorganic Chemistry

journal homepage: www.elsevier.com/locate/bioorg

Evaluation of cytotoxic activity and genotoxicity of structurally well characterized potent cobalt(II) phen–based antitumor drug entities: An *in vitro* and *in vivo* approach

Huzaifa Yasir Khan[a], Mohd Owais Ansari[b], G.G.H.A. Shadab[b], Sartaj Tabassum[a], Farukh Arjmand[a,*]

[a] Department of Chemistry, Aligarh Muslim University, Aligarh 202002, Uttar Pradesh, India
[b] Cytogenetics and Molecular Toxicology Laboratory, Section of Genetics, Department of Zoology, Aligarh Muslim University, Aligarh 202002, Uttar Pradesh, India

ARTICLE INFO

Keywords:
Gel electrophoresis
In silico molecular docking
In vitro DNA binding
Cyclic voltammetry
Cytotoxicity

ABSTRACT

Cobalt (II) phen–based drug candidates of the formulation $Co(phen)_2Cl_2$, **1**, $Co(phen)_2L$, **2** where L = 1*H*–pyrazole–3,5–dicarboxylic acid were synthesized and thoroughly characterized by spectroscopic methods and single X–ray crystallography. DNA binding interaction of **1** and **2** was carried out employing biophysical techniques {UV–visible, fluorescence, thermal denaturation and cyclic voltammetry} to validate their potential to act as antitumor agents. The interpretations of these biophysical studies of **1** and **2** supported the non–covalent intercalative binding mode; furthermore, a higher binding trend of **2** was observed as compared to **1**, phen and 1*H*–pyrazole–3,5–dicarboxylic acid alone. Cleavage studies of **1** and **2** with pBR322 were assessed by gel electrophoresis and it was observed that both drug candidates cleave DNA by hydrolytic pathway involving hydroxyl radical (˙OH). Cytotoxic activity of **1** and **2** against human cancer cell lines [MCF–7 (breast), HeLa (cervical), MIA–PA–CA 2 (pancreatic), A–498 (kidney), Hep–G2 (hepatoma)] was evaluated by SRB assay. The obtained results showed that drug candidate **1** showed significantly low GI_{50} value (< 10 μg/ml) against MCF–7 and HeLa cell lines. However, candidate **2** revealed excellent cytotoxicity (< 10 μg/ml) against all the tested cancer cell lines. The *in vivo* genotoxicity of **2** was evaluated by micronucleus (MN) test and chromosomal aberration (CA) in bone marrow cells of the Wistar rats to check cobalt(II)–induced systemic toxicity. The results showed that no significant chromosomal aberrations and micronucleus formation was observed at 5 mg/kg and 10 mg/kg in presence of drug candidate **2** implicating that it could be administered safely at a low dosage. However, an elevated percentage of chromosomal aberration and micronucleated polychromatic erythrocytes (MNPCE) was observed only at higher doses (20 mg/kg and 40 mg/kg) of drug candidate **2**.

1. Introduction

Medicinal inorganic chemistry, also coined as “Elemental medicine” is a younger discipline of bioinorganic chemistry pertaining to the use of transition metals for preparation of new pharmaceuticals for the treatment of diseases ranging from cardiovascular, diabetes, respiratory disorders, HIV/AIDS and cancers [1]. Transition metals are endowed with unique spectroscopic and physicochemical properties *viz*., strong Lewis acidity, variable oxidation states, unsaturated coordination environments, a wide array of geometric possibilities from tetragonal, trigonal bipyramidal to octahedral etc; in addition to thermodynamic and ligand field stabilities of their complexes [2]. Many late 3d–transition metal ions viz., Fe(II), Co(II), Cu(II) and Zn(II) have been explored for their chemotherapeutic properties for cancers and some of the metallo–drugs have also entered clinical trials, namely a family of copper complexes under the registered name Casiopeinas® of the formulation $[Cu(NN)(NO)]NO_3$ where the NN ligand denotes either 2,2’–bipyridine or 1,10–phenanthroline (the aromatic ligand) and NO is an essential amino acid or peptides has been found to be active towards a myriad range of tumors [3]. Similarly, cobalt–based peptide drug candidate, Marismastat demonstrated significant antineoplastic activity [4]. The advances in therapeutic metallo–drugs have appeared in many review articles, which describe the understanding of the active structure/pharmacophore of the drug entities, behaviour in the biological

Abbreviations: Phen, phenanthroline; SEM, scanning electron microscope; MCF–7, breast cancer cell line; HeLa, cervical cancer cell line; MIA–PA–CA 2, pancreatic cell line; A–498, kidney carcinoma cell line; Hep–G2, hepatoma cancer cell line

* Corresponding author.
E-mail address: farukh.arjmand18@gmail.com (F. Arjmand).

https://doi.org/10.1016/j.bioorg.2019.102963
Received 29 January 2019; Received in revised form 25 April 2019; Accepted 28 April 2019
Available online 02 May 2019

environment, or the exact molecular mechanism of action at the target site *in vitro* and *in vivo* [5–7]. These transition metal complexes have also been explored as metallonucleases as they can utilize their open coordination positions for DNA binding and hydrolysis which could generate reactive oxygen–containing species or other radicals responsible for DNA oxidation [8].

Since transition metals are amenable to complexation with a diverse range of organic ligands such as Schiff bases, amino acids, flavonoids, N–heterocycles (1,10–phenanthroline and bipyridine) and pyrazolones etc, therefore, several drug–like molecules with different biological profile can be achieved which offer enhanced pharmacological response at the molecular level. Previous literature report reveals that the pharmacological activity depends on the nature of metal ion and the ligand scaffold [9]. Moreover, chelating ligands present in the complexes play a key role in i) muting the toxicity of metal ion ii) and to increase the lipophilic character of the organic scaffold [10].

Cobalt is an essential redox trace element which exists in three favourable oxidation states, Co(I), Co(II) and Co(III) and play a profound role in vitamin B_{12} (alkyl cobalamin) chemistry participating in many redox, alkylation and radical–induced reactions in the living system [7]. The cytotoxic potential of cobalt complexes arises due to the redox behaviour of cobalt as activation of cobalt(III) in a hypoxic environment by reduction to cobalt(II) and release of ligand, and generation of reactive oxygen species (ROS) by the catalytic auto–oxidation process [11]. Furthermore, cobalt(II) complexes have been extensively investigated for hydrolytic DNA cleaving ability [12]. Efficacious metallonucleases can be designed based on the strategy of finding a metal ion and an intercalating scaffold such as 1,10–phen. Complexes containing 1,10–phen have emerged as potential therapeutic agents due to its conformational rigidity, charge density, lipophilicity and pharmacological advantages as metabolic stability [13]. Colak *et al* reported the cytotoxic activity of cobalt–phen complex conjugated with dicarboxylic acid moiety on rat glioma (C6) cells. The results showed that the complex was less toxic compared to free ligand [14].

In continuation to our interest to design and synthesize potential metal–based anticancer chemotherapeutic drug candidates in our laboratory, herein, we have utilized late 3d–transition metal ion, cobalt(II) to furnish new drug entities from biologically significant heterocyclic *N,Ń* donor, 1,10–phenanthroline and 1*H*–pyrazole–3,5–dicarboxylic acid ligand scaffolds. *In vitro* cytotoxicity evaluation of **1** and **2** against human cancer cell lines were analyzed to validate their chemotherapeutic potential. The *in vivo* genotoxic potential of synthesized drug **2** was evaluated by chromosomal aberrations and micronucleus (MN) test on bone marrow cells in Wistar rats to optimize the safe dosage of synthesized drug candidate.

2. Experimental

2.1. Materials and instrumentation

1*H*–pyrazole–3,5–dicarboxylic acid, 1,10–phenanthroline (Sigma Aldrich), KOH and $CoCl_2{\cdot}6H_2O$ (Merck) were purchased and used as received. Supercoiled pBR322 plasmid DNA, HSA and 5′–GMP were procured from Fisher Scientific and were utilized as received. Colchicine (CAS 64–86–8), Cyclophosphamide (CAS 6055–19–2), Giemsa stain and May–Gruenwald stain were purchased from Merck, India. Fetal Bovine Serum (FBS) was procured from Gibco by life technologies, India. All other chemicals and solvents used were of analytical grade. Elemental analysis was carried out on a Carlo Erba Analyser Model 1106. Infrared spectra were obtained (KBr disk, 400–4000 cm^{-1}) on a Perkin–Elmer Model 1320 spectrometer. Scanning electron microscope (SEM) was recorded on Zeiss supra 55VP scanning electron microscope. Electronic spectra were recorded on a Perkin–Elmer Lambda 25 using cuvettes of 1 cm path length, and the data were reported in λ_{max}/nm. Magnetic properties of complexes **1** and **2** were determined by the Evans method using magnetic susceptibility balance (Sherwood scientific). Emission spectra were acquired on a Shimadzu RF–5301PC spectrofluorophotometer. The TGA analysis of complexes **1** and **2** was performed on Schimadzu DTG-60H analyzer under nitrogen atmosphere from 20 to 850 °C at a heating rate of 20 °C/min.

In vitro DNA binding studies were performed in Tris–HCl buffer (pH = 7.3) and the DNA concentration was determined by the UV absorbance at 260 nm using $\varepsilon = 6600\ M^{-1}cm^{-1}$conformed to the standard methods previously adopted by our laboratory [15].

The thermal denaturation measurements were carried out using a Perkin Elmer Lambda 850 spectrophotometer equipped with a Peltier temperature controlling programmer.

Cyclic voltammetry was carried out at CH instrument electrochemical analyzer. High purity H_2O and DMSO (95:5) was employed for the cyclic voltammetry studies with 0.4 M KNO_3 as a supporting electrolyte. A three electrode configuration was used comprising of a Pt disk working electrode, Pt wire counter electrode and Ag/AgCl as reference electrode. Electrochemical measurements were made under N_2 atmosphere.

Cleavage experiments were performed with the help of Axygen electrophoresis supported by a Geneipower supply with a potential range of 50–500 V, and visualized by vilber–INFINITY gel documentation system.

2.2. Syntheses

2.2.1. Synthesis of $[Co(phen)_2Cl_2]$, 1

Complex **1** was prepared by the slight modification of Garai *et al* [16] employing a straightforward reaction of methanolic solutions of 1,10–phenanthroline and $CoCl_2{\cdot}6H_2O$ in 2:1 M ratio. Slow evaporation of reaction mixture yielded single crystals suitable for X–ray crystallography. The complex **1** was pure and soluble in DMF and DMSO.

$[Co(phen)_2Cl_2]$, **1**: Yield: 75%, m.p. 265 °C; CCDC: 1826438, anal. Calc. for $[C_{24}H_{16}Cl_2CoN_4]$ (%): C, 58.80; H, 3.29; N, 11.43; Found: C, 58.53; H, 3.09; N, 10.72. UV–vis (1×10^{-4} M, DMSO, λ_{max}nm): 305 (π–π*), 342 (n–π*), 558 (d–d). FT–IR (KBr pallet, υ_{max}/cm^{-1}):1581 ν(C═N), 590 ν(Co–N), 430 ν(Co–O).

2.2.2. Synthesis of $[Co(phen)_2L]$, 2

The complex **2** was synthesized by modification of Xie *et al* method [17]. Complex **2** was prepared by carrying out the reaction of 1, 10–phenanthroline, $CoCl_2{\cdot}6H_2O$ and 1*H*–pyrazole–3,5–dicarboxylic acid (in the presence of KOH) in 2:1:1 M ratio. The product was isolated by evaporation of reaction mixture after the completion of reaction which was monitored on TLC. Single crystals suitable for X–ray crystallography were obtained at room temperature.

$[Co(phen)_2L]$, **2**: Yield: 76%, m.p. > 300 °C; CCDC: 1817080, anal. Calc. for $[C_{29}H_{18}CoN_6O_4]$ (%): C, 60.74; H, 3.16; N, 14.66; Found: C, 60.68; H, 3.23; N, 14.23. UV–vis (1×10^{-4} M, DMSO, λ_{max} nm): 261 (π–π*), 330 (n–π*), 573 (d–d). FT–IR (KBr pallet, υ_{max}/cm^{-1}):1689, 1647 ν(C═O), 1572 ν(C═N), 1519 ν(C═C), 594 ν(Co–N), 426 ν(Co–O).

2.3. X–ray diffraction studies

Single crystal X–ray data for cobalt (II) phen–based drug candidates **1** and **2** were collected on a Bruker SMART APEX CCD diffractometer (100 K) using graphite monochromatic Mo–Kα radiation (k = 0.71073 Å). The linear absorption coefficients, scattering factors for the atoms and the anomalous dispersion corrections were referred from the International Tables for X–ray Crystallography. The data integration and reduction were carried out with SAINT software. Empirical absorption correction was applied to the collected reflections with SADABS program [18] and the space group was determined using XPREP. The structure was solved by direct methods using SHELXTL–97 and refined on F2 by full–matrix least–squares using the SHELXTL–97 programme package [19]. A summary of selected crystallographic information is given in Table 1.

Table 1
Crystallographic data for cobalt (II) phen–based drug candidates **1** and **2**.

Parameters	1	2
CCDC	1,826,438	1,817,080
Formula	$C_{24}H_{16}Cl_2CoN_4$	$C_{29}H_{18}CoN_6O_4$
Fw (g mol^{-1})	490	573
crystal system	monoclinic	monoclinic
space group	*C2/c*	*C2/c*
a (Å)	15.2280(7)	25.5296(8)
b (Å)	13.4285(7)	16.3043(8)
c (Å)	12.1870(6)	16.0790(6)
α (deg)	90	90
β(deg)	99.353(2)	113.053(1)
γ (deg)	90	90
U ($Å^3$)	2459.0(2)	6158.3(4)
ρ_{calc} (g/cm^3)	1.324	1.237
Z	4	8
μ (mm^{-1})	0.932	0.598
Temp (K)	100 K	296 K
Measured reflns	18,211	46,365
Indep reflns	1942	4720
GoF[a]	1.052	1.068
R[b] [I > 2σ (I)]	0.0365	0.0500
wR_2[b] (all data)	0.1175	0.1572

[a] GoF is defined as $\{\Sigma[w(F_0^2 - F_c^2)]/(n - P)\}^{1/2}$ where n is the number of data and p is the number of parameters.
[b] $R = \{\Sigma||F_0| - |F_c||/\Sigma|F_0|$, $wR^2 = \{\Sigma\, w(F_0^2 - F_c^2)^2/\Sigma\, w(F_0^2)^2\}^{1/2}$.

2.4. Cytotoxicity evaluation

The cytotoxic activity of cobalt (II) phen–based drug candidate **1** was evaluated against three human cancer cell lines *viz.*, MIA–PACA–2 (Pancreatic), MCF–7 (breast) and HeLa (cervical) while in case of **2**, A–498 (Renal cell) and Hep–G2 (Hepatoma) cell lines in addition to MIA–PACA–2 (Pancreatic), MCF–7 (breast) and HeLa (cervical) were chosen for evaluation by SRB assay. Adriamycin, standard anticancer drug was taken as positive control. The cell lines were grown in RPMI 1640 medium containing 10% fetal bovine serum and 2 mM L–glutamine. For present screening experiment, cells were inoculated into 96 well microtiter plates in 100 μl at plating densities as shown in the study details above, depending on the doubling time of individual cell lines. After cell inoculation, the microtiter plates were incubated at 37 °C, 5% CO_2, 95% air and 100% relative humidity for 24 h prior to addition of **1** and **2**. Drug candidates **1** and **2** were initially solubilized in dimethyl sulfoxide at 100 mg/ml and diluted to 1 mg/ml using water and stored frozen prior to use. At the time of drug addition, an aliquot of frozen concentrate (1 mg/ml) was thawed and diluted to 100 μg/ml, 200 μg/ml, 400 μg/ml and 800 μg/ml with complete medium containing test article. Aliquots of 10 μl of these different drug dilutions were added to the appropriate microtiter wells already containing 90 μl of medium, resulting in the required final drug concentrations *i.e.* 10 μg/ml, 20 μg/ml, 40 μg/ml, 80 μg/ml. After addition of drug candidates **1** and **2**, plates were incubated at standard conditions for 48 h and assay was terminated by the addition of cold TCA. Cells were fixed *in situ* by the gentle addition of 50 μl of cold 30% (w/v) TCA (final concentration, 10% TCA) and incubated for 60 min at 4 °C. The supernatant was discarded; the plates were washed five times with tap water and air dried. Sulforhodamine B (SRB) solution (50 μl) at 0.4% (w/v) in 1% acetic acid was added to each of the wells, and plates were incubated for 20 min at room temperature. After staining, unbound dye was recovered and the residual dye was removed by washing five times with 1% acetic acid. The plates were air dried. Bound stain was subsequently eluted with 10 mM trizma base, and the absorbance was read on an plate reader at a wavelength of 540 nm with 690 nm reference wavelength. Percent growth was calculated on a plate–by–plate basis for test wells relative to control wells. Percent growth was expressed as the ratio of average absorbance of the test well to the average absorbance of the control wells * 100. Using the six absorbance measurements [time zero (T_z), control growth (C), and test growth in the presence of drug at the four concentration levels (T_i)], the percentage growth was calculated at each of the drug concentration levels. Percentage growth inhibition was calculated as: [Ti/C] × 100% [20].

2.5. Molecular docking

Molecular docking studies were performed using HEX 8.0 software [21], an interactive molecular graphics program for calculating and displaying feasible docking modes of enzymes and DNA molecules. Visualization of the docked pose was performed using the Discovery Studio molecular graphics program.

2.6. Animals and treatment

The model animal for the study were male Wistar rats (*Rattus norvegicus*), weighing 100 ± 120 g. The animals were given rat diet and water ad libitum in standard laboratory condition with room temperature of 18–25 °C, relative humidity 45–55% and, 12/12 h of light/dark cycle. Before treatment, the animals were acclimatized with the standard laboratory conditions for about 15 days. All the experiments were carried out in strict compliance with ethical principles of institutional animal committee and guidelines provided by "committee for the purpose of control and supervision of experiments on animals"(CPCSEA). The study was approved by the Committee for the Advance Studies and Research (CASR). The experimental protocol was approved by institutional animal ethics committee, Aligarh Muslim University, Aligarh, India. Animals were divided in six different groups with six animals in each group ($n = 6$). The drug candidate **2** was dissolved in DMSO and was given intraperitonially (i.p.). Group 1st and 2nd group served as negative control and positive control (cyclophosphamide, 40 mg/kg). The 3rd to 6th group were given 5 mg/kg, 10 mg/kg, 20 mg/kg, 40 mg/kg of the test compound, respectively.

2.7. Cytogenetic analysis

2.7.1. Chromosomal aberration (CA) assay

The metaphase chromosomes were prepared as par the modified protocol of Shadab *et al.* [22] Simply, after the treatment, the rats were sacrificed and femur bones were taken out. The bone marrow was flushed out in test tubes with pre–warmed 0.075 M KCl and centrifuged at 300 g for 10 min. Again, the pellets were mixed with KCl and left in water–bath (37 °C) for 20 min. for hypotonic treatment. After centrifugation, the pellets were kept and mixed with freshly prepared fixative (methanol: glacial acetic acid, 3:1) and left for overnight (preferably). Again, the samples were centrifuged and the remaining pellets were resuspended in fixative. Slides were prepared by dropping the sample on pre–chilled slides tilted at an angle of 45° and left for air dry. After that slides were stained with 5% Giemsa stain, mounted in DPX and were analyzed under light microscope (Nikon, Japan) at 100X immersion oil lens. 600 cells per group were counted and used for calculation of mean number of chromosomal aberration.

2.7.2. Micronucleus test (MNT)

Micronucleus test was done as per the methods of Schmidt [23] with slight modification by Parveen and Shadab [24]. After 24 h of treatment, rats were sacrificed and the femur bones were taken out. Next, the bone marrow was flushed out with fetal bovine serum (FBS) using insulin syringe and centrifuged at 100 g for 10 min. After, centrifugation, pellets were mixed thoroughly, smears were drawn on clean slides and left for air dry. Next, the slides were stained with May–Gruenwald stain followed by Giemsa stain and mounted in DPX before analyzing under microscope. The mean number of micronucleus polychromatic erythrocytes (MNPCEs) per 2000 polychromatic erythrocytes (PCEs) were used for calculations.

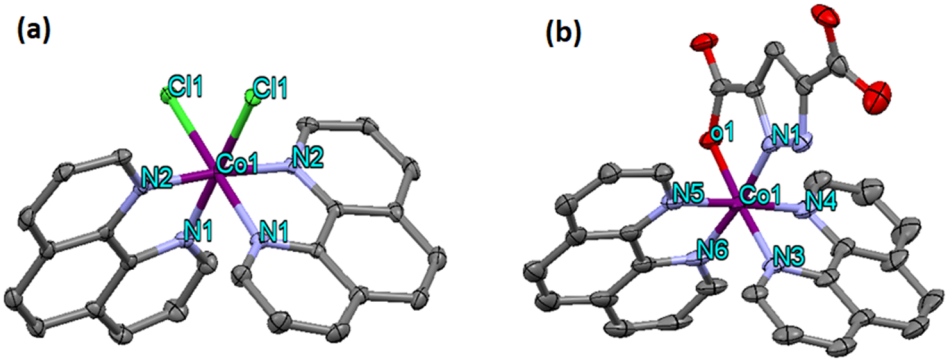

Fig. 1. ORTEP diagram of drug candidates (a) **1** and (b) **2** with partial numbering. Hydrogen atoms have been omitted for clarity.

3. Results and discussion

3.1. Synthesis and characterization

Cobalt (II) phen–based complexes **1** and **2** were synthesized as promising antitumor chemotherapeutic drug candidates and thoroughly characterized by elemental analysis and other spectroscopic methods. The molecular structures were established by single crystals X–ray diffraction studies. All synthesized complexes were found to be stable towards air and soluble in organic solvents like DMF and DMSO.

3.2. Spectroscopic measurements

The IR spectrum of complex **1** exhibited characteristic ν(C═N) band of 1,10–phenanthroline at 1605 cm^{-1}which on complexation undergoes an appreciable blue shift to 1563 cm^{-1} implicating the coordination of metal through bidentate two nitrogen atoms of phen. The complex **2** showed strong bands at1689 and 1647 cm^{-1} for asymmetric stretching and at 1464 and 1431 cm^{-1} for symmetric stretching, respectively attributed to presence of two carboxylic acid groups in 1*H*–pyrazole–3,5–dicarboxylic acid [25]. The vibrational frequencies of ν(C═N) and ν(C═C) at 1605 cm^{-1} and 1500 cm^{-1} corresponding to phenanthroline ligand were shifted on coordination to 1572 and 1519 cm^{-1}, respectively [26]. The supportive evidence for the coordination of metal in complexes **1** and **2** was ascertained by the appearance of ν(Co−N) and ν(Co−O) bands at *ca.* 595–427 and 563–425 cm^{-1} in the far IR region [27].

The electronic spectrum of the complex **1** displayed two strong absorption bands centred at 305 nm and 342 nm ascribed to the π–π* or n–π* transitions in the pyridine rings of phenanthroline ligands and a broad band at 558 nm attributed to $^4T_{1g}(F) \rightarrow {}^4T_{1g}(P)$ transition indicative of high spin octahedral Co(II) environment. The absorption spectrum of complex **2** revealeda weaker broad envelope at 573 nm attributed to octahedral Co(II) ion which was followed by strong spectral bands in the UV region at 261 nm and 330 nm assigned to the π–π* and n–π* ligand centred transitions [28].

The effective magnetic moment of complexes **1** and **2** was calculated at room temperature by the equation $\mu_{eff} = 2.828\ [\chi_m T]^{1/2}$ (where χ_m is the molar susceptibility and *T* is the absolute temperature), which was found to be 4.54 and 4.65B.M, respectively. These values were higher than the spin–only value expected for a high spin d^7 ion (S = 3/2, 3.87B.M.) and are consistent with three unpaired electron for Co(II) complexes in an octahedral geometry [29].

3.3. Thermal analysis

To examine the thermal stability of complexes **1** and **2**, thermogravimetric analysis was performed in a temperature range of 20–800 °C. The TGA curves (Fig. S4) indicated the weight loss in three steps over temperature range, 95–140, 220–400 and 450–800 °C. For complexes **1** and **2**, the first step demonstrated the loss of lattice water accompanied by a weight loss of 14.30% and 15.02% (calculated %: 13.90 and 14.88), respectively. In the second step for **1** and **2** as temperature increased, further weight loss of 30.78% and 31.65% (calculated %: 30.44% and 30.81%), respectively, occurred in the temperature range 220–400 °C corresponding to loss of 1,10–phenanthroline ligands. Finally in the third step, further weight loss of 23.34% and 24.59% (calculated %: 23.36 and 24.70), respectively, in the temperature range of 450–800 °C was assigned to loss of chlorine molecules for complex **1** and 1*H*–pyrazole–3,5–dicarboxylic acid ligand in case of complex **2** thereby leading to formation of cobalt oxide (Co_3O_4) as a residue.

3.4. Single X–ray crystal description

The molecular structure of cobalt (II) phen–based drug candidates **1** and **2** along with the atom numbering scheme is shown in Fig. 1. Both the structures crystallize in monoclinic crystal system with *C*2/*c* space groups, the metal atoms lie on a symmetry centre. In complex **1**, Co(II) atom is coordinated to four nitrogen atoms (N1–N4) from two phenanthroline ligands and two chlorine atoms form an octahedral geometry possessing lattice parameters, a = 15.2280(7) Å, b = 13.4285(7) Å, c = 12.1870(6) Å, $\alpha = \gamma = 90^0$, β = 99.353(2)^0. The bite angle Cl (1)–Co(1)–Cl(1) (91.96^0) indicates the *cis* conformation of the structure. The asymmetric unit of complex **2** revealed a distorted octahedral coordination geometry, in which 1*H*–pyrazole–3,5–dicarboxylic acid and phenanthroline ligands bind in chelating mode. The central Co(II) ion exhibited distorted octahedral geometry by coordination to pyrazole N atom, carboxylate O atom viz., Co(1)–N(1) = 1.879 Å, Co(1)–O (1) = 1.905 Å and four nitrogen atoms (N3–N6) of two phenanthroline ligands *viz.*, Co(1)–N(3) = 1.934(3) Å, Co(1)–N(4) = 1.928(3) Å, Co (1)–N(5) = 1.930(3) Å, Co(1)–N(6) = 1.957(3) Å. The space group lattice parameters were found to be, a = 25.52(8) Å, b = 16.30(8) Å, c = 16.07(6) Å with $\alpha = \gamma = 90^0$, β = 113.053^0. The crystal structure was further stabilized by intermolecular hydrogen bonding interactions (Fig. 2.) as well as π–π* stacking interaction involving centrosymmetrically oriented aromatic rings through the carbon atoms *viz.*, C10…C14, C12…C12 and C14…C10. The selected bond length and angles of **1** and **2** have been listed in Tables S1 and S2.

3.5. Binding profile of cobalt(II) phen–based drug candidates with ct–DNA

Interaction studies of cobalt(II) phen–based drug entities **1** and **2** with ct–DNA were analyzed by various biophysical techniques *viz.*, UV–vis, fluorescence, thermal denaturation and cyclic voltammetry to ascertain their potential to act as chemotherapeutic drug entities. The UV–vis spectral titrations of drug candidates were recorded at a fixed concentration (0.067 × 10^{-4} M) of drug candidates and varying conc. (0.067–0.4 × 10^{-4} M) of ct–DNA (Fig. 3). With increasing aliquots of ct–DNA, a “hypochromism”(55% for **1** and 68% for **2**) at intraligand

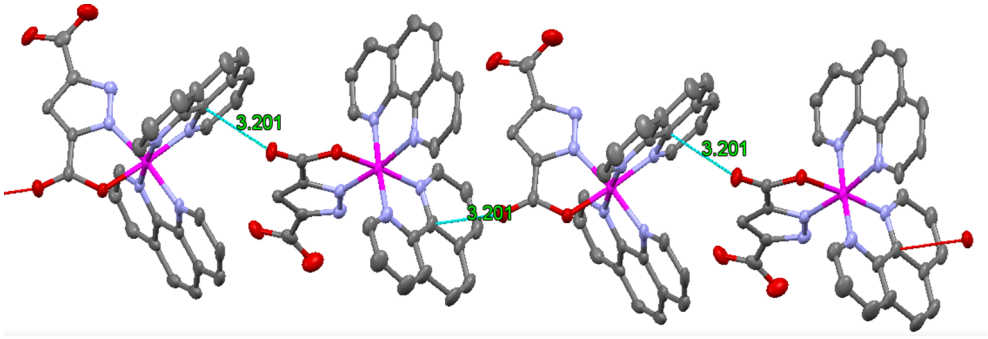

Fig. 2. Packing diagram of cobalt (II) phen–based drug candidate **2** showing intermolecular hydrogen bonding.

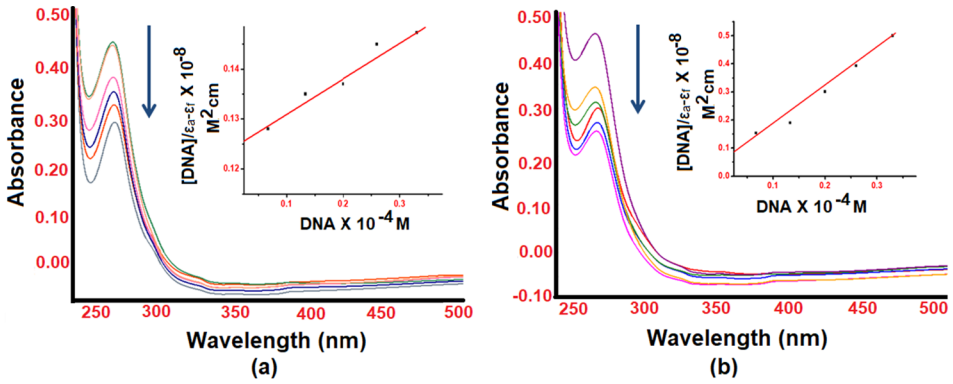

Fig. 3. Absorption spectra of drug candidates **(a) 1** and **(b) 2** in Tris–HCl buffer at pH 7.2 upon addition of increasing amounts of ct–DNA.

absorption band (260 nm) was observed for both the drug candidates revealing non–covalent intercalative mode of binding which involves π–π stacking interactions between the aromatic planar chromophore of the candidates and base pairs of DNA [30]. Intercalation is of paramount importance in the design of metallated drugs, where planar heterocyclic systems can actually 'wedge' between the base pairs of duplex DNA, causing the unwinding of the DNA localized at the site of intercalation. This is highly specific regio–selective approach of cell death and first step in inhibiting gene expression [31].

The binding strength of the free ligands namely, 1,10–phenanthroline and 1*H*–pyrazole–3,5–dicarboxylic acid and the drug candidates **1** & **2** was quantified by determining the intrinsic binding constant K_b values as shown in Table 2. The K_b values demonstrated higher binding propensity of complex **2** as compared to **1** and the corresponding free ligand moieties. The higher DNA binding affinity of **2** could be attributed to the presence of an extended aromatic pyrazole ring which facilitates effective interaction with DNA base pairs through hydrogen bonding interactions.

An optically sensitive fluorescence method was selected to further ascertain whether the cobalt(II) phen–based drug candidates could exhibit binding at the DNA double helix and to validate the recognition of intercalating mode of complexes. The emission spectra of drug candidates **1** and **2** exhibited appreciable fluorescence at 362 nm in Tris–HCl buffer (pH 7.2) at room temperature in the absence of ct–DNA upon excitation at 261 nm. On titrating **1** and **2** (0.067×10^{-4} M) with increasing aliquots of ct–DNA ($0–4 \times 10^{-5}$), emission intensity decreased progressively. (Fig. S1) This quenching phenomenon in emission intensity in presence of candidates **1** and **2** is suggestive of intercalation with double–stranded DNA [32]. The binding constant *K* of the free ligands viz., 1,10–phenanthroline & 1*H*–pyrazole–3,5–dicarboxylic acid and the drug candidates **1** & **2**, derived from Scatchard equation [33] was calculated to be $1.69(\pm 0.02) \times 10^4$ and $1.5(\pm 0.05) \times 10^4$, $2.7\ (\pm 0.10) \times 10^4$ and $1.4\ (\pm 0.05) \times 10^5$ M^{-1}, respectively, consistent with results of absorption spectral titrations.

To further authenticate the intercalative mode of the drug candidates with ct–DNA, competitive binding experiments based on the displacement of intercalating drug EB from DNA were carried out. The emission spectra of EB–DNA system in presence and in the absence of drug candidates **1** and **2** are depicted in Fig. 4. On addition of increasing concentration of drug candidates ($0–0.4 \times 10^{-4}$ M) to the fixed concentration of ct–DNA penetrated with EB, there was a significant reduction in the emission intensity. The quenching plots of *I0/I* vs [complex **1**/**2**]/[DNA] (insets of Fig. 4) are in well agreement with the linear Stern–volmer equation [34]. Stern–volmer quenching constants (K_{sv}) were calculated as 0.74, 1.83, 0.64 and 0.62 for complexes **1, 2** and the free ligands namely, 1,10–phenanthroline and 1*H*–pyrazole–3,5–dicarboxylic acid, respectively.

The interaction of cobalt(II) phen–based drug candidates **1** and **2** with ct–DNA was further investigated by measuring the changes in the DNA melting temperature (T_m). As ds–DNA is heated slowly, the helix

Table 2
Binding Parameters of cobalt(II) phen–based drug candidates with ct–DNA.

Drug candidates	K_b (M^{-1})	K (M^{-1})	K_{sv}
1	$3.60(\pm 0.05) \times 10^4$	$2.70(\pm 0.10) \times 10^4$	0.74
2	$1.19(\pm 0.02) \times 10^5$	$1.40(\pm 0.05) \times 10^5$	1.83
1,10–phen	$2.10(\pm 0.04) \times 10^4$	$1.69(\pm 0.02) \times 10^4$	0.64
1*H*–pyrazole–3,5–dicarboxylic acid	$1.90(\pm 0.10) \times 10^4$	$1.50(\pm 0.05) \times 10^4$	0.62

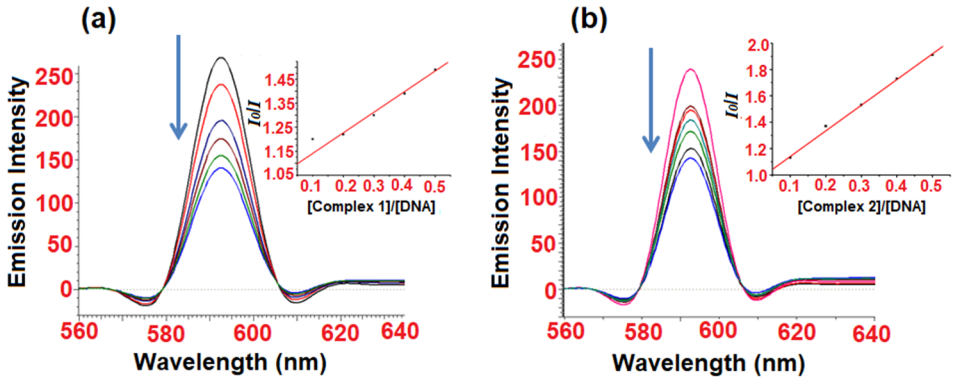

Fig. 4. Emission spectra of drug candidates (a) **1** and (b) **2** in Tris HCl buffer at pH 7.2 upon addition of ct–DNA.

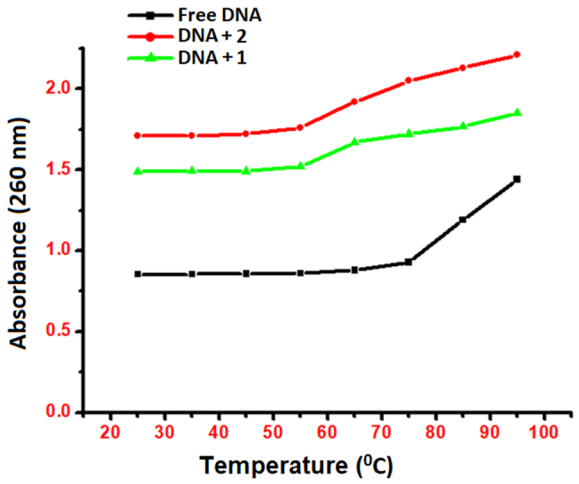

Fig. 5. Thermal denaturation profile of ct–DNA before and after addition of cobalt(II) phen–based drug candidates **1** and **2** (80 μM).

unfolds and the interaction between the base pairs of the helix decreases to give single stranded DNA. The temperature (T_m) at which 50% of double–stranded DNA denatured into single stranded one was calculated from the mid–point of DNA melting curve (λ_{ex} = 260 nm). Literature revealed that groove or electrostatic binding through negatively–charged oxygen atoms of the phosphate backbone of DNA results only a small change in DNA melting temperature. However, intercalation leads to a high value of the same due to the stabilization of the DNA duplex [35]. In our experiments, an appreciable change (10 °C) in T_m value was observed revealing binding of both the drug candidates **1** and **2** predominantly *via* intercalation (Fig. 5).

The electrochemical investigations of drug–DNA interaction were carried out in DMSO solution at room temperature at a scan rate of 0.2 Vs^{-1} by cyclic voltammetry in the potential range of −1 to 1 V. Generally, the electrochemical potential of drug candidate shifts to more negative value upon electrostatic interaction with DNA while a positive shift will be observed in case of intercalative mode of binding [36].

The cyclic voltammetric behaviour of cobalt(II) phen–based drug candidates in the absence and in presence of ct–DNA is depicted in Fig. 6. The CV of **2** demonstrated a quasi–reversible one electron redox process involving Co(II)/Co(I) couple with a cathodic peak at E_{pc} = –0.75 V and an anodic peak at E_{pa} = –0.125 V. For this couple, the difference between cathodic and anodic potential $\Delta E_p$was found to be –0.625 V. The formal electrode potential $E_{1/2}$, as an average of E_{pc} and E_{pa} was –0.43 V in the absence of ct–DNA. The CV of **1** featured reduction of Co(II)/Co(I) form at a cathodic peak potential of E_{pc} = –0.68 V and an oxidation peak appeared at E_{pa} = –0.27 V. The difference between both the peak potential was found to be –0.41 V.

Addition of ct–DNA to the drug candidate **2** resulted in much significant reduction in the cathodic and anodic peak currents due to the slow diffusion of an equilibrium mixture of the free and DNA–bound drug candidates to the electrode surface; however less significant changes were observed in both the currents for **1** as compared to **2**, validating higher DNA binding propensity of **2**. The observed shifts in $E_{1/2}$ values towards more positive value ascertain an intercalative mode of binding well–corroborated with results of other spectroscopic techniques.

The electrochemical behaviour of drug candidate **2** was further studied with different molecules of biological interest viz., nucleotide (guanosine mono phosphate; 5′–GMP) and proteins such as human serum albumin (HSA).

Addition of HSA to the drug candidate **2** resulted in significant reduction in cathodic and anodic peak currents due to the slow diffusion of an equilibrium mixture of free and HSA bound complex to the electrode surface. On the other hand, on addition of nucleotide (5′–GMP) to the drug candidate **2**, significant reduction in the cathodic peak current was observed. The observed shift in E_{pa} and E_{pc} value (Fig. 7) indicate that both Co(II) and Co (I) forms bind to HSA/5′–GMP with good affinity. Furthermore, the addition of HSA to the solution of **2** shows an apparent decrease in the Co(II)/Co(I) reduction peak current due to the formation of adducts with lower diffusion coefficients. [37]

3.6. Morphological studies

Recently, controllable drug–DNA condensation has shown much enormous prospectus for transportation of drug candidates across the biological membranes to specific target at the molecular level [38]. The cationic molecules exhibit tendency to condense DNA and form DNA condensates of spherical morphology which have ability to enhance the efficiency of gene transfer *in vitro* and *in vivo* [39]. The molecular interactions between DNA and the cationic component determine many vital biological processes *viz.*, recombination, replication transcription and repair [40]. These include enhancement of cell membrane interactions due to electrostatic forces, increased cellular uptake by endocytosis, and improved trafficking to the nucleus [41]. Morphology of DNA condensates vary with the change in solution properties (ionic strength and solvent polarity), nature of condensing agent (charge density) and the surface of substrate [42]. In this experiment, DNA condensate of drug candidate **1** and **2** was prepared by evaporating an equimolar mixture of **1**, **2** and ct–DNA in Tris–HCl buffer. Scanning electron microscope (SEM) was employed to observe the morphological changes of DNA–drug candidate **1**/DNA–drug candidate **2** condensates as compared to **1** and **2** alone. The SEM micrographs of **1** and **2** displayed crystalline and irregular morphologies in case of **1**, while **2** revealed concrete rock–like structures. (Fig. 8) The region of DNA condensate of drug candidates **1** and **2** are encircled in Fig. 8(b,d) which showed that DNA condensate of drug candidate **1** represented mixing of

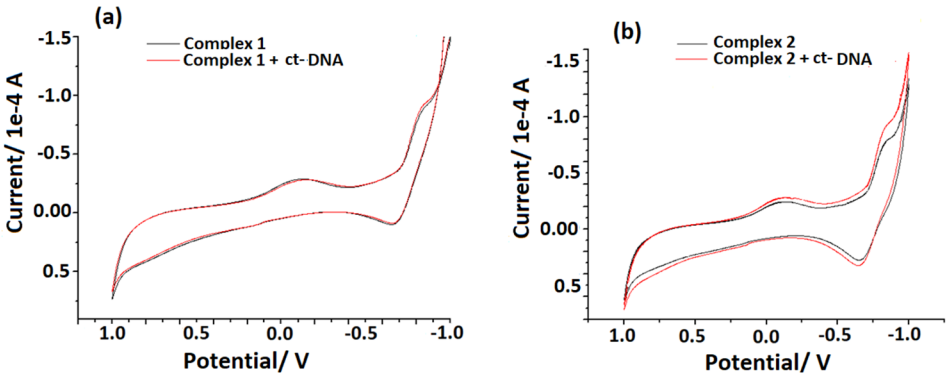

Fig. 6. Cyclic voltammogram (1:2 DMSO: buffer solution, 25 °C) of drug candidates **1** and **2** in the absence and presence of ct–DNA at a scan rate = 0.2 Vs^{-1}.

complex and DNA particles. On the other hand, DNA condensate of **2** showed some rod–shaped structures and DNA particles were randomly distributed over them. The results of DNA condensates suggest the interaction of cobalt(II) phen–based drug candidates with ct–DNA has occurred, followed by lengthening of DNA double helix with the insertion of complexes **1** and **2** inside the DNA base pairs [43]. It was also observed that **2** demonstrated more prominent morphological changes compared to **1** with ct–DNA.

3.7. Chemical nuclease activity

The ability of cobalt(II)phen–based drug candidates to serve as metallonucleases was ascertained by gel electrophoresis on plasmid pBR322 DNA as a substrate in a medium of 5 mM Tris–HCl/50 mM NaCl buffer at physiological pH and temperature. On incubation of the drug candidates **1** and **2** with the plasmid DNA, the naturally occurring supercoiled form (Form I) showed the fastest migration. When one strand of the plasmid DNA is cleaved, Form I relaxes to produce a slower–moving nicked circular form (Form II) whereas Form III migrates between Form I and Form II in case of double stranded cleavage [44]. The results of concentration dependent cleavage experiment (in the range of 5–50 μM) of plasmid DNA by the complexes **1** & **2** are depicted in Fig. 9(a) & Fig. 10(a). The cobalt(II) phen–based drug candidate **1** exhibited significant cleavage at 45 μM while in case of **2** efficient cleavage was observed at a very low concentration of 10 μM. These results are in agreement with other spectroscopic DNA binding experiments which suggest higher binding trend of **2** as compared to **1**.

To elucidate the mechanistic pathway of cleavage process, cleavage reactions of drug candidates **1** and **2** were carried out in presence of standard additives such as DMSO, EtOH (˙OH) scavenger, NaN_3($^1O_2$) scavenger, and SOD ($˙O_2^-$). The drug candidate **1** showed good inhibition in presence of hydroxyl radical scavenger DMSO while complete inhibition of nuclease activity was observed in presence of both DMSO and EtOH (lanes 6 and 7) in case of **2** suggesting the involvement of diffusible (˙OH) hydroxyl radical as one of the reactive oxygen species implicating that the DNA damage was mediated via hydrolytic cleavage pathway. However, the cleavage process remained unaffected in presence of NaN_3 and SOD for drug candidate **1** ruling out the possibility of involvement of singlet oxygen $^1O_2$ and superoxide $˙O_2^-$ scavengers (lanes 8 and 9). The drug candidate **2** showed partial inhibition in presence of SOD but markedly significant inhibition with NaN_3 strongly supportive of the involvement of singlet oxygen ROS. Furthermore, the effect of activators *viz.*, H_2O_2, Asc (ascorbate), 3–mercaptopropionic acid (MPA), and glutathione (GSH) on the cleavage activity were also studied and it was observed that they followed the order H_2O_2 > GSH > Asc ~ MPA and H_2O_2 > Asc > MPA > GSH for drug candidates **1** and **2**, respectively.

The groove binding preference of the drug candidates **1** and **2** was examined in presence of groove binders, minor groove (DAPI) and major groove (MG). As shown in Fig. 9(b) and Fig. 10(b), the cleavage of DNA was slightly diminished for both the drug candidates in presence of minor groove DAPI (lanes 10 and 11) validating their interaction through minor surface groove of DNA helix.

The cleavage pattern revealed that both the drug candidates **1** and **2** followed similar cleavage mechanism involving hydroxyl radicals, resulting in the hydrolytic cleavage of the sugar phosphate backbone of the DNA [45]. Generally, hydrolytic pathway depends on the Lewis acidity of the central metal ion which results in the activation of phosphodiester bonds towards nucleophilic attack *via* charge neutralisation and thereby leads to direct hydrolysis of the diester bonds [46]. In our drug

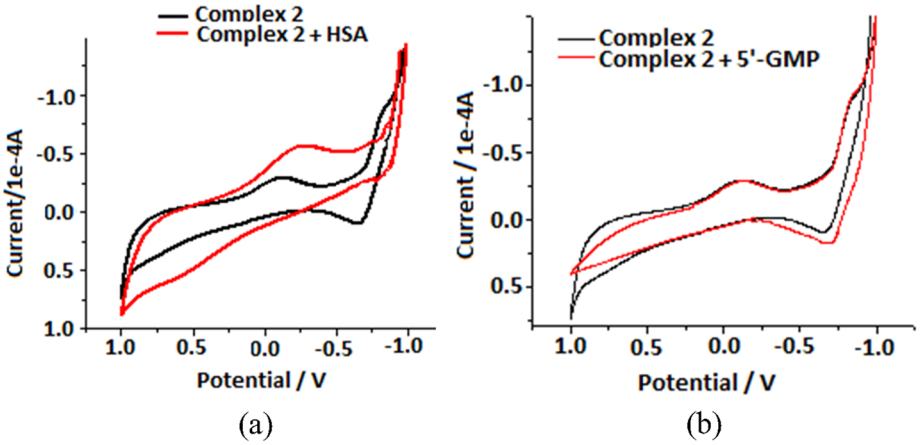

Fig. 7. Cyclic voltammogram (1:2 DMSO: buffer solution, 25 °C) of drug candidates **1** and **2** in the absence and presence of (a) HSA (b) 5′-GMP at a scan rate = 0.2 Vs^{-1}.

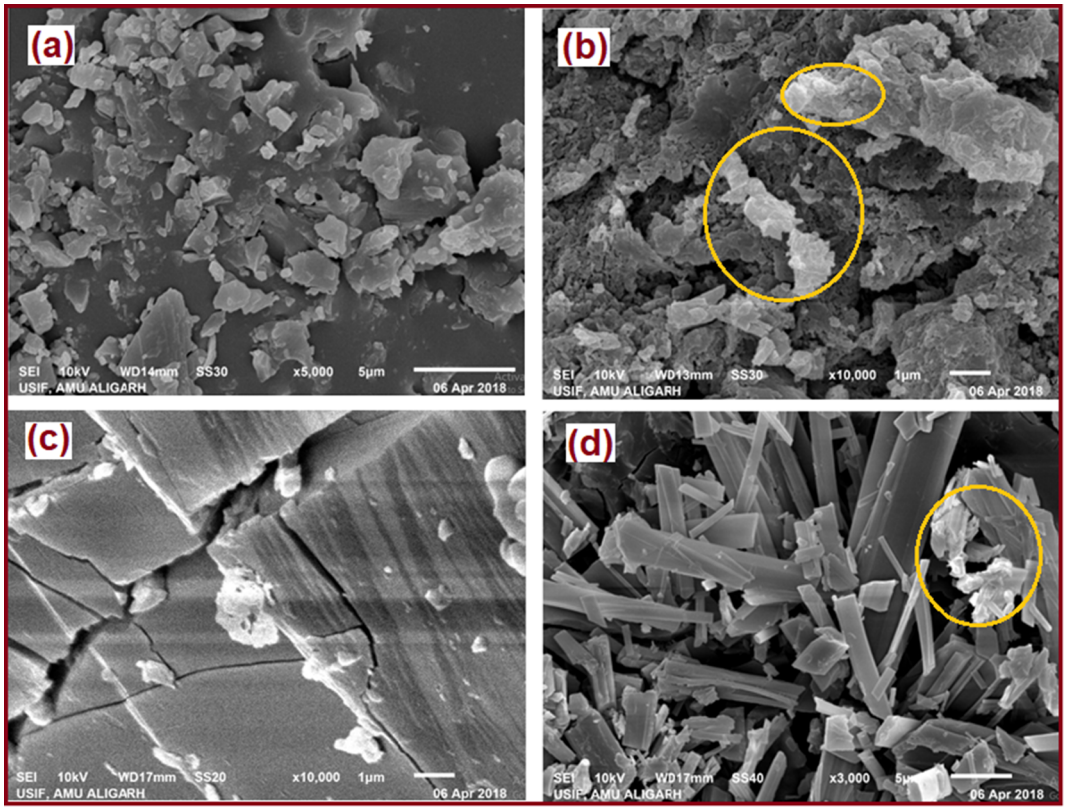

Fig. 8. Scanning electron micrographs showing morphology of drug candidate (a) **1** & (c) **2** alone and (b) **1** & (d) **2** upon interaction with ct–DNA.

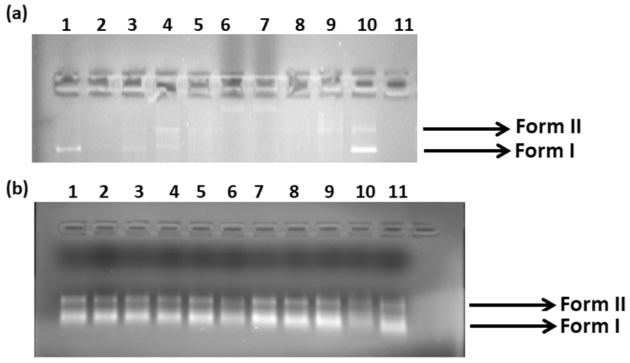

Fig. 9. The cleavage patterns of pBR322 supercoiled DNA (300 ng) observed in gel electrophoresis by drug candidate **1** at 37 °C kept for 30 min of incubation time; **(a)** Lane 1: DNA control; Lane 2: 5 μM of **1** + DNA; Lane 3: 10 μM of **1** + DNA; Lane 4: 15 μM of **1** + DNA; Lane 5: 20 μM of **1** + DNA; Lane 6: 25 μM of **1** + DNA; Lane 7: 30 μM of **1** + DNA; Lane 8: 35 μM of **1** + DNA; Lane 9: 40 μM of **1** + DNA; Lane 10: 45 μM of **1** + DNA; Lane 11: 50 μM of **1** + DNA; **(b)** Lane 1: DNA control; Lane 2: 45 μM of **1** + H_2O_2 (0.4 mM) + DNA; Lane 3:45 μM of **1** + MPA (0.4 mM) + DNA; Lane 4:45 μM of **1** + Asc (0.4 mM) + DNA; Lane 5:45 μM of **1** + GSH (0.4 mM) + DNA; Lane 6:45 μM of **1** + DMSO (0.4 mM) + DNA; Lane 7:45 μM of **1** + Ethyl alcohol (0.4 mM) + DNA; Lane 8: 45 μM of **1** + SOD (15 U) + DNA; Lane 9:45 μM of **1** + DNA + NaN_3(0.4 mM); Lane 10:45 μM of **1** + DNA + DAPI (8 μM); Lane 11:45 μM of **1** + DNA + MG (2.5 μM of a 0.01 mg/ml solution).

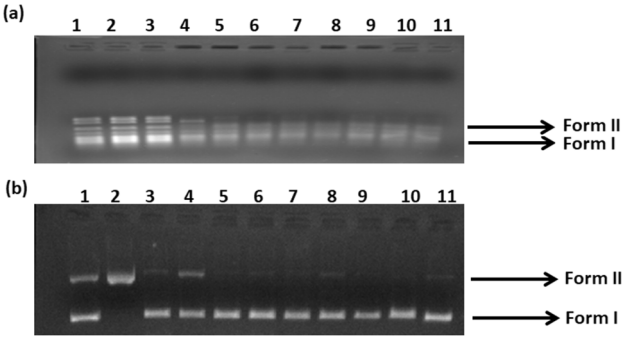

Fig. 10. The cleavage patterns of pBR322 supercoiled DNA (300 ng) observed in gel electrophoresis by drug candidate **2** at 37 °C kept for 30 min of incubation time; **(a)** Lane 1: DNA control; Lane 2: 5 μM of **2** + DNA; Lane 3: 10 μM of **2** + DNA; Lane 4: 15 μM of **2** + DNA; Lane 5: 20 μM of **2** + DNA; Lane 6: 25 μM of **2** + DNA; Lane 7: 30 μM of **2** + DNA; Lane 8: 35 μM of **2** + DNA; Lane 9: 40 μM of **2** + DNA; Lane 10: 45 μM of **2** + DNA; Lane 11: 50 μM of **2** + DNA; **(b)** Lane 1: DNA control; Lane 2: 10 μM of **2** + H_2O_2 (0.4 mM) + DNA; Lane 3:10 μM of **2** + MPA (0.4 mM) + DNA; Lane 4:10 μM of **2** + Asc (0.4 mM) + DNA; Lane 5:10 μM of **2** + GSH + DNA; Lane 6:10 μM of **2** + DMSO (0.4 mM) + DNA; Lane 7:10 μM of **2** + EtOH (0.4 mM) + DNA; Lane 8: 10 μM of **2** + SOD (15 U) (0.4 mM) + DNA; Lane 9:10 μM of **2** + DNA + NaN_3 (0.4 mM); Lane 10:10 μM of **2** + DNA + DAPI (8 μM); Lane 11:10 μM of **2** + DNA + MG (2.5 μM of a 0.01 mg/ml solution).

candidates, cobalt synergistically with planar *N,N′* aromatic ligand mediates the hydrolytic cleavage of DNA helix [47].

3.8. *In silico* molecular docking studies

In silico molecular docking is a crucial process to understand the drug–DNA interactions which can substantiate our experimental results. Docked ligand conformation was analyzed in terms of energy and hydrophobic interaction with drug candidates and B–DNA (PDB ID = 1BNA). From the docking scores, the free energy of binding of drug candidates was calculated and results are shown in Table 3.

In silico molecular docking results revealed that both the drug candidates **1** and **2** fitted snugly into the DNA intercalative sites or the curved contour of the targeted DNA in the narrow and slightly deeper G–C region of the minor groove. The candidate **1** was found in the close

Table 3
The calculated free energy of binding of Co(II) phen–based drug candidates with B–DNA (1BNA).

Drug candidates	Binding energy (kJ mol^{-1})
1	–275
2	–300

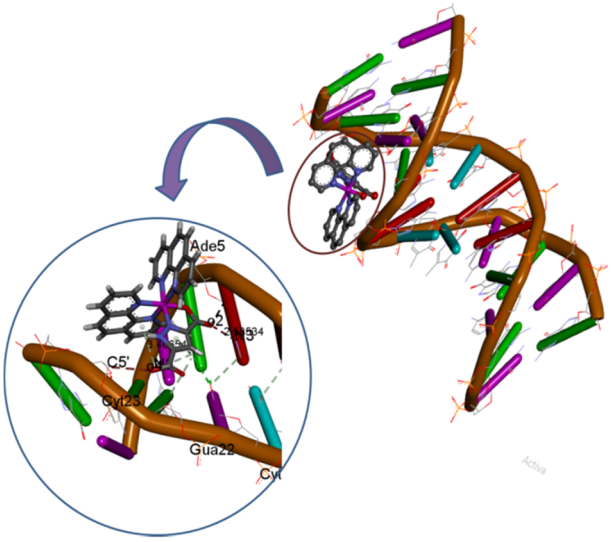

Fig. 11. Molecular docked model of drug candidate **2** fitted into the G–C region of minor groove of DNA along with possible hydrogen bonding interactions with the base pairs.

proximity of C21, G22, T20, C3, G4, A5 and A6 DNA base pairs (Fig. S2). On the other hand, drug candidate **2** interacts *via* C23, C21, G22, A5 DNA base pairs in such a way that aromatic rings make favourable stacking interaction between DNA base pairs. The carbonyl oxygen atoms (O2 and O4) from two dicarboxylate moiety form hydrogen bond with the nitrogen atom of A5 (DA5: N3….O2 = 2.585 Å) and hydrogen atom of C23 (DC 23: H….O4 = 3.46 Å) DNA base pairs, respectively. (Fig. 11) The results obtained in terms of free energy of binding and hydrophobic interaction correlate well with other experimental

Table 4
Anticancer activity of Co(II) phen–based drug candidates as a panel of human cancer cell lines in terms of GI_{50} (μg/ml) values.

Cell lines	MCF-7	HeLa	MIA-PA-CA 2	HepG2	A-498
1	< 10	< 10	NE		–
2	< 10	< 10	< 10	< 10	< 10
ADR	< 10	< 10	< 10	< 10	< 10

GI_{50} = growth inhibition of 50% (GI_{50}) calculated from $[(T_i - T_z)/(C - T_z)] \times 100 = 50$, drug concentration that results in a 50% reduction in the net protein increase.
ADR = Adriamycin (positive control).

spectroscopic techniques suggesting drug candidate **2** possess a higher binding ability.(See. Fig. 12.)

3.9. In vitro cytotoxic evaluation

In vitro cytotoxic activity of cobalt–phen based drug candidate **1** was evaluated against three human cancer cell lines viz., MCF–7 (breast), HeLa (cervix) and MIA–PA–CA 2 (Pancreas) while candidate **2** was evaluated against MCF–7 (breast), HeLa (cervix), MIA–PA–CA 2 (Pancreas), A–498 (Kidney) and Hep–G2 (Hepatoma) cancer cell lines by SRB assay. The drug candidate **1** with bis(phen) recognition domain chelated to cobalt ion, engaged in strong π–π* stacking intercalation binding affinity exhibited profoundly good cytotoxic activity with GI_{50} value (< 10 μg/ml) against two cancer cell lines viz., MCF–7 and HeLa. The candidate **2,** on the other hand demonstrated much superior and wider spectrum of cytotoxicity (< 10 μg/ml) against all the tested cancer cell lines (Table 4) as compared to **1**, attributed to the presence of an efficient biologically active ligand moiety, 1*H*–pyrazole–3,5–dicarboxylic acid which induces p–π* conjugation due to its extended planar structure on chelation with central cobalt ion [48]. The morphological changes observed in these cell lines exposed to complex **2** for a period of 48 h demonstrated that a reduction in morphology, as well as cell adhesion capacity was observed as compared to control drug (Fig. S3)

3.10. Cytogenetic analysis

The mean frequency chromosomal aberration (CA) is also used to evaluate the genotoxicity of the drug candidate. In our experiments, we observed chromosomal aberration in the form of chromosome breaks,

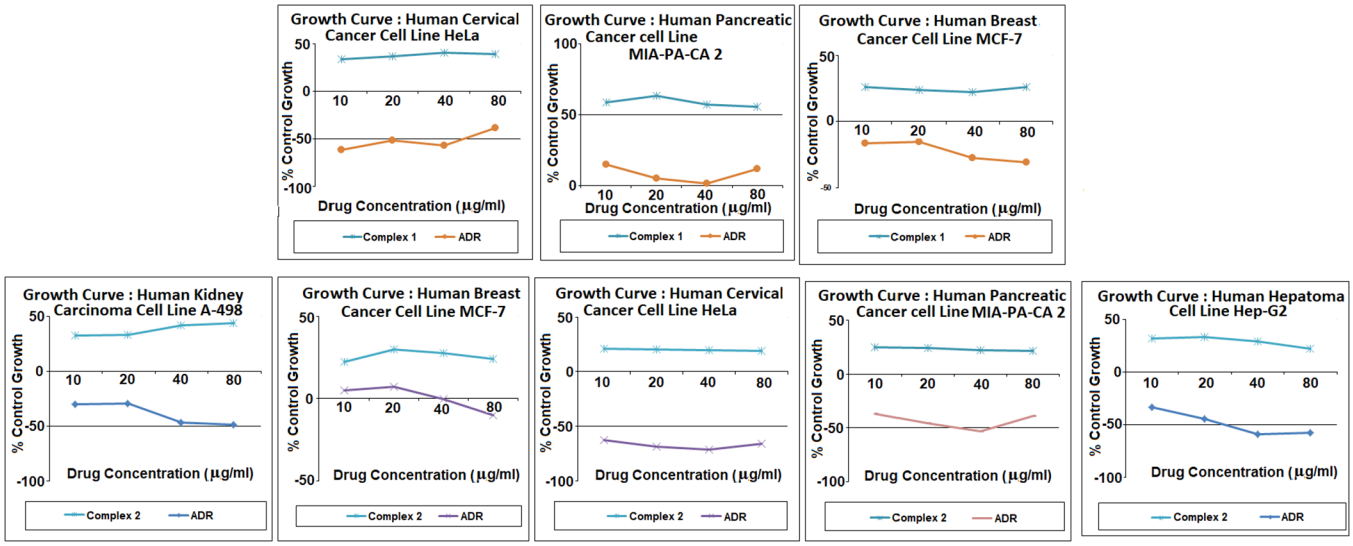

Fig. 12. Growth curve showing % control growth verses drug concentration (μg/ml) of **1** and **2** against different human carcinoma cell lines.

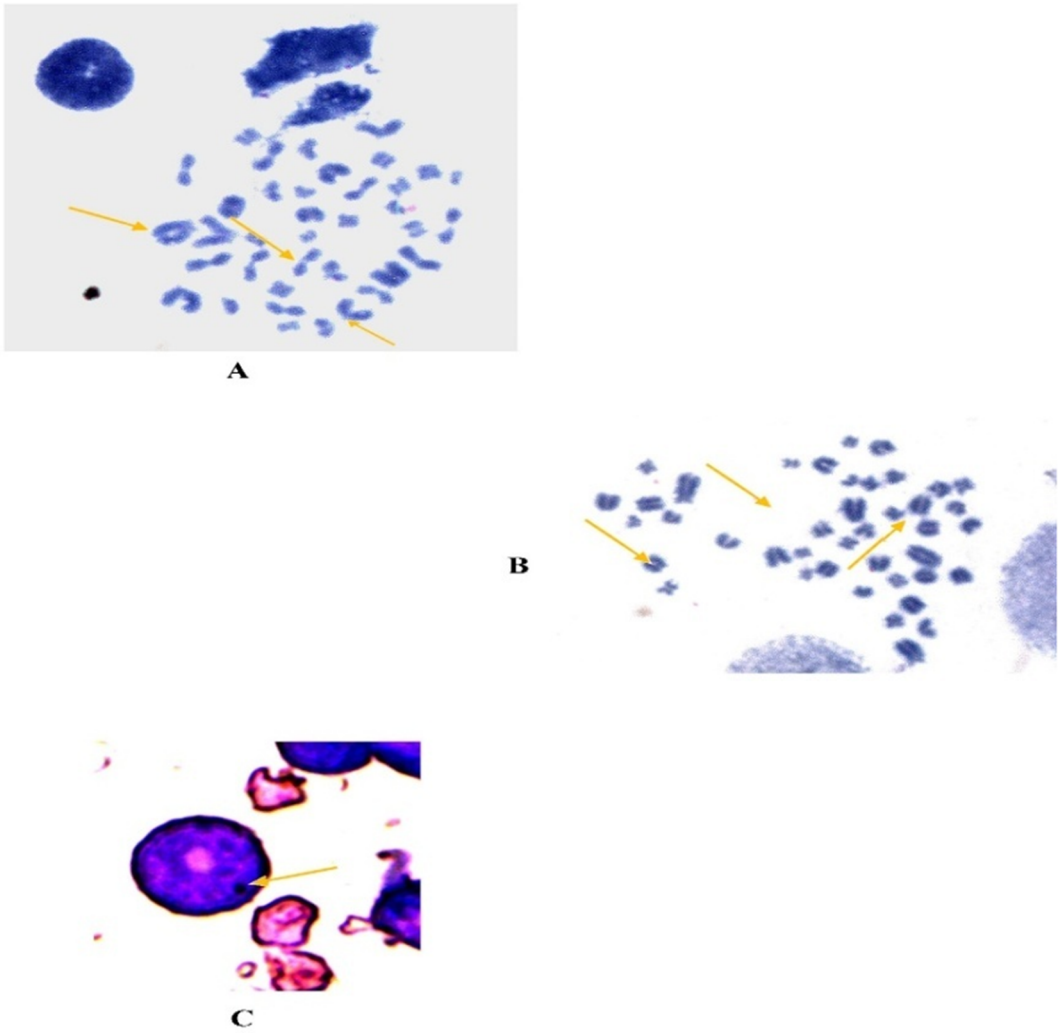

Fig. 13. Photographs showing chromatid breaks, chromosome breaks, acentric fragments and chromosomal ring (**A-B**); micronucleus in polychromatic erythrocytes (**C**).

chromatid breaks, acentric fragments and chromosomal rings (Fig. 13). The mean number of CA were calculated per 600 cells after the treatment of drugs. From the data obtained, the mean number of CA were found to be 81.33 ± 7.50 (positive control), 1.33 ± 0.49 (negative control), 2.83 ± 0.70 (5 mg/kg), 5.50 ± 2.66 (10 mg/kg), 14.66 ± 3.98 (20 mg/kg) and 35.16 ± 2.56 (40 mg/kg) respectively (Fig. 14A). The obtained data showed that at 5 mg/kg and 10 mg/kg, there was no statistically significant differences as compared to control. However, at 20 mg/kg and 40 mg/kg, statistically significant increase ($^{*}p < 0.05$) in CA frequency was observed as compared to control, though the mean frequency was found to be low as compared to positive control.

Similarly, Micronucleus (MN) induction is a potential marker of genotoxicity assessment of pharmaceutical drug entity. The mean number of MNPCEs (micronucleus polychromatic erythrocytes) among 2000 PCEs (polychromatic erythrocytes) was used to evaluate the genotoxic potential of the compound. From the obtained data, the mean number of MNPCEs were found to be 39.83 ± 5.30 (positive control), 0.83 ± 0.75 (negative control), 2.16 ± 0.75 (5 mg/kg), 4.33 ± 1.86 (10 mg/kg), 9.50 ± 1.86 (20 mg/kg), 17.66 ± 2.16 (40 mg/kg) respectively (Fig. 14B). Statistical analysis showed that at 5 mg/kg and 10 mg/kg, there is no significant increase in MNPCEs as compared to control. However, with the increase in dose (20 mg/kg and 40 mg/kg), there was a significant increase in MNPCEs (statistical significance level set at $^{*}p < 0.05$). The observed genotoxicity in the form of chromosomal aberration and micronucleus induction might be due to the oxidative stress induced by the drug candidates.

4. Conclusion

Cobalt (II) phen–based drug candidates **1** and **2** were synthesized as promising antitumor chemotherapeutics as validated by *in vitro* DNA binding profile and cytotoxicity activity on a panel of human cancer cell lines. *In vivo* genotoxicity of **2** in healthy Wistar rats was performed to establish their safe administration and toxicity profile. Both the drug candidates were thoroughly characterized and the structure was fully elucidated by single crystal X–ray studies which depicted distorted octahedral geometry of these drug entities around Co(II) centre. *In vitro* DNA interaction studies of these drug candidates showed that candidates bind to DNA *via* intercalative mode and the drug candidate **2** demonstrated a higher binding propensity as compared to **1** and their corresponding free ligands, respectively. Cleavage studies of **1** and **2** with pBR322 DNA were assessed by gel electrophoresis and it was observed that both drug candidates cleave DNA by hydrolytic pathway involving hydroxyl radical species. Validation of antitumor potential of **1** and **2** was done by cytotoxicity experiments against human cancer cell lines. Drug candidate **1** showed significantly low GI_{50} value (< 10 μg/ml) against MCF–7 and HeLa cell lines while candidate **2** revealed excellent cytotoxicity (< 10 μg/ml) against all the tested

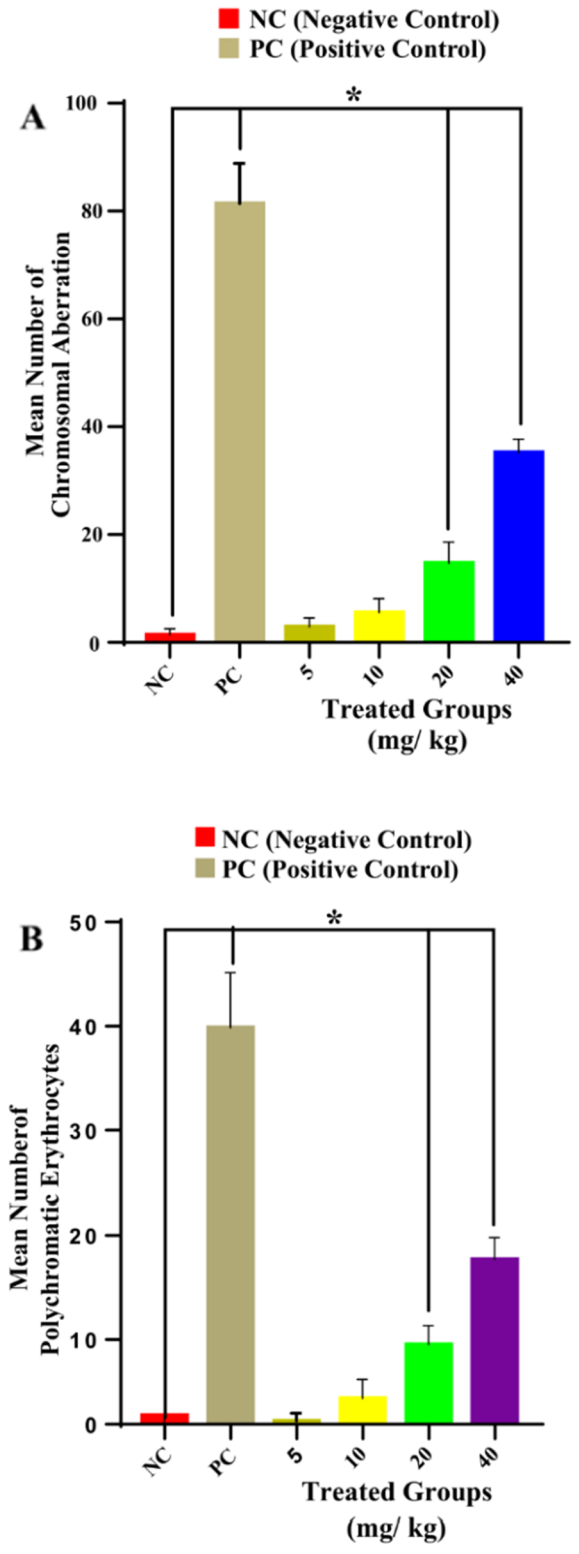

Fig. 14. Graph showing the mean number of chromosomal aberration **(A)** and mean number of micronucleus in polychromatic erythrocytes **(B)** after 24 h of drug treatment. One-way ANOVA was used for analysis of data. All values as expressed as mean ± SD. Statistical significance level was set at $^{*}p < 0.05$.

cancer cell lines. The genotoxicity of drug candidate **2** was evaluated *in vivo* by micronucleus (MN) testing and chromosomal aberration on bone marrow cells of the Wistar rats. These results showed that the drug candidate **2** could be safely administered at a low drug concentration, however higher dosage of drug candidate **2** results in slight percent elevation of micronucleated polychromatic erythrocytes. The corroborative results demonstrated that the cobalt (II) phen–based drug candidate **2** can act as a promising anticancer drug candidate with considerable *in vivo* genotoxic activity and warrant its further biological investigation.

Acknowledgement

The author (Huzaifa Yasir Khan) gratefully acknowledges financial support from Department of Science and Technology, New Delhi for providing DST–INSPIRE Senior Research Fellowship (DST/AORC–IF/UPGRD/IF160130). The authors extend thanks to Dr. Musheer Ahmad, Department of Applied Chemistry, Aligarh Muslim University, Aligarh for refining single X–ray crystal data of complexes and IIT Kanpur for solving the structures. The authors also extend their appreciation to the University Sophisticated Instruments Facility (USIF) and Instrumentation Centre, Department of Chemistry, Aligarh Muslim University, Aligarh for respective analysis. The authors are highly thankful to anticancer drugs screening facility (ACDSF) of ACTREC, Tata Memorial Centre, Navi Mumbai for carrying out *in vitro* anti-cancer activity of complexes by SRB assay. M.O. Ansari and G. G. H. A. Shadab are gratefully acknowledged for carrying out genotoxicity of synthesized complexes.

Appendix A. Supplementary material

Supplementary data to this article can be found online at https://doi.org/10.1016/j.bioorg.2019.102963.

References

[1] Z. Guo, P.J. Sadler, Metals in medicine, Angew. Chemie Int. Ed. 38 (1999) 1512–1531.
[2] G. Kumaravel, P.P. Utthra, N. Raman, Exploiting the biological efficacy of benzimidazole based Schiff base complexes with l-Histidine as a co-ligand: Combined molecular docking, DNA interaction, antimicrobial and cytotoxic studies, Bioorg. Chem. 77 (2018) 269–279.
[3] R. Galindo-Murillo, J.C. García-Ramos, L. Ruiz-Azuara, T.E. Cheatham, F. Cortés-Guzmán, Intercalation processes of copper complexes in DNA, Nucl. Acids Res. 43 (2015) 5364–5376.
[4] S.R. Bramhall, M.T. Hallissey, J. Whiting, J. Scholefield, G. Tierney, R.C. Stuart, R.E. Hawkins, P. McCullock, T. Maughan, P.D. Brown, M. Baillet, Marimastat as maintenance therapy for patients with advanced gastric cancer: a randomised trial, Brit. J. Cancer. 86 (2002) 1864–1870.
[5] K.D. Mjos, C. Orvig, Metallodrugs in medicinal inorganic chemistry, Chem. Rev. 114 (2014) 4540–4563.
[6] W.A. Wani, S. Prashar, S. Shreaz, S. Gomez-Ruiz, Nanostructured materials functionalized with metal complexes: In search of alternatives for administering anticancer metallodrugs, Coord. Chem. Rev. 312 (2016) 67–98.
[7] C.R. Munteanu, K. Suntharalingam, Advances in cobalt complexes as anticancer agents, Dalt. Trans. 44 (2015) 13796–13808.
[8] L.E. Scott, C. Orvig, Medicinal inorganic chemistry approaches to passivation and removal of aberrant metal ions in disease, Chem. Rev. 109 (2009) 4885–4910.
[9] S. Tabassum, M. Zaki, F. Arjmand, I. Ahmad, Synthesis of heterobimetallic complexes: In vitro DNA binding, cleavage and antimicrobial studies, J. Photochem. Photobiol. B Biol. 114 (2012) 108–118.
[10] M. Selvaganapathy, N. Raman, Pharmacological activity of a few transition metal complexes: A short review, J. Chem. Biol. Ther. (2016) 1–17.
[11] S. Osinsky, I. Levitin, L. Bubnovskaya, A. Sigan, I. Ganusevich, A. Kovelskaya, N. Valkovskaya, L. Campanella, P. Wardman, Selectivity of effects of redox-active cobalt (III) complexes on tumor tissue, Exp Oncol. 26 (2004) 140–144.
[12] (a) T.F.S. Silva, L.M. Martins, M.F.C.G. da Silva, A.R. Fernandes, A. Silva, P.M. Borralho, S. Santos, C.M.P. Rodrigues, A.J.L. Pombeiro, Cobalt complexes bearing scorpionate ligands: synthesis, characterization, cytotoxicity and DNA cleavage, Dalt. Trans. 41 (2012) 12888–12897;
(b) M. Ahmad, M. Afzal, S. Tabassum, B. Kalińska, J. Mrozinski, P.K. Bharadwaj, Synthesis and structure elucidation of a cobalt (II) complex as topoisomerase I inhibitor: In vitro DNA binding, nuclease and RBC hemolysis, Eur. J. Med. Chem. 74 (2014) 683–693.
[13] S. Marcaccini, R. Pepino, M.C. Pozo, S. Basurto, M. García-Valverde, T. Torroba, One-pot synthesis of quinolin-2-(1H)-ones via tandem Ugi-Knoevenagel condensations, Tetrahedron Lett. 45 (2004) 3999–4001.
[14] A.T. Colak, P. Oztopcu-Vatan, F. Colak, D. Akduman, S. Kabadere, R. Uyar, Syntheses, characterization, antimicrobial and cytotoxic activities of pyridine-2, 5-dicarboxylate complexes with 1, 10-phenanthroline, J. Trace Elem. Med. Biol. 27 (2013) 295–301.

[15] (a) F. Arjmand, M. Muddassir, Y. Zaidi, D. Ray, Design, synthesis and crystal structure determination of dinuclear copper-based potential chemotherapeutic drug entities; in vitro DNA binding, cleavage studies and an evaluati, Med. Chem. Comm. 4 (2013) 394–405;
(b) I. Yousuf, F. Arjmand, S. Tabassum, L. Toupet, R.A. Khan, M.A. Siddiqui, Mechanistic insights into a novel chromone-appended Cu (II) anticancer drug entity: in vitro binding profile with DNA/RNA substrates and cytotoxic activity against MCF–7 and HepG2 cancer cells, Dalt. Trans. 44 (2015) 10330–10342.

[16] M. Garai, D. Dey, H.R. Yadav, M. Maji, A.R. Choudhury, B. Biswas, Synthesis and phosphatase activity of a Cobalt (II) phenanthroline complex, J. Chem. Sci. 129 (2017) 1513–1520.

[17] H. Xie, C. Xie, G. Shen, D. Shen, X. Wang, (5–Carboxy–1H–pyrazole–3–carboxylato–κ2N2, O3) bis (1, 10–phenanthroline–κ2N, N′) cobalt (III) perchlorate 2.5–hydrate, Acta Crystallogr. Sect. E. 63 (2007) m1477–m1479.

[18] Software Users Guide, v. 6.0, Bruker Analytical X–ray Systems, Madison, WI, (1999); G.M. Sheldrick, SADABS: Area − Detector Absorption Correction, v. 2.03, University of Gottingen, Gottingen, Germany, (1999); SADABS, v. 2008.

[19] G.M. Sheldrick, SHELXL–97, Progr, Crystal-Structure Refinement, 1997.

[20] (a) V. Vichai, K. Kirtikara, Sulforhodamine B colorimetric assay for cytotoxicity screening, Nat. Protoc. 1 (2006) 1112–1116;
(b) P. Skehan, R. Storeng, D. Scudiero, A. Monks, J. McMahon, D. Vistica, J.T. Warren, H. Bokesch, S. Kenney, M.R. Boyd, New colorimetric cytotoxicity assay for anticancer-drug screening, JNCI J. Natl. Cancer Inst. 82 (1990) 1107–1112.

[21] G. Macindoe, L. Mavridis, V. Venkatraman, M.-D. Devignes, D.W. Ritchie, HexServer: an FFT–based protein docking server powered by graphics processors, Nucl. Acids Res. 38 (2010) W445–W449.

[22] G. Shadab, M.E. Ahmad, M. Afzal, Effect of hydrocortisone on human lymphocyte chromosomes *in vitro*, Indian Biol. 31 (1999) 1–10.

[23] W. Schmid, The micronucleus test, Mutat. Res. 31 (1975) 9–15.

[24] N. Parveen, G.G. Shadab, The dual clastogenic and anti-clastogenic properties of quercetin is dose dependent, Front. Biosci. (Schol. Ed). 9 (2017) 139–153.

[25] M.-L. Cheng, W. Han, Q. Liu, J.-T. Bao, Z.-F. Li, L.-T. Chen, X.-Q. Sun, H.-T. Xi, Synthesis, crystal structures, and luminescent properties of Pb (II) and Sr (II) coordination polymers constructed by 5-methyl-1H-pyrazole-3-carboxylic acid, J. Coord. Chem. 67 (2014) 215–226.

[26] J. Yang, J.-F. Ma, D.-M. Wu, L.-P. Guo, J.-F. Liu, Syntheses, crystal structures and characterization of divalent transition metal sulfonate complexes with o–phenanthroline, J. Mol. Struct. 657 (2003) 333–341.

[27] K. Nakmoto, Infrared and Raman spectra of Inorganic and Coordination Compounds: Part A, fifth ed., John Wiley & Sons Inc., New York, 1997.

[28] F.E. Jacobsen, R.M. Breece, W.K. Myers, D.L. Tierney, S.M. Cohen, Model complexes of cobalt-substituted matrix metalloproteinases: Tools for inhibitor design, Inorg. Chem. 45 (2006) 7306–7315.

[29] F. Lloret, M. Julve, J. Cano, R. Ruiz-García, E. Pardo, Magnetic properties of six-coordinated high-spin cobalt (II) complexes: Theoretical background and its application, Inorganica Chim. Acta. 361 (2008) 3432–3445.

[30] M. Baldini, M. Belicchi-Ferrari, F. Bisceglie, P.P. Dall'Aglio, G. Pelosi, S. Pinelli, P. Tarasconi, Copper (II) complexes with substituted thiosemicarbazones of α-ketoglutaric acid: synthesis, X-ray structures, DNA binding studies, and nuclease and biological activity, Inorg. Chem. 43 (2004) 7170–7179.

[31] A.C. Komor, J.K. Barton, The path for metal complexes to a DNA target, Chem. Commun. 49 (2013) 3617–3630.

[32] N. Shahabadi, S. Kashanian, F. Darabi, DNA binding and DNA cleavage studies of a water soluble cobalt (II) complex containing dinitrogen Schiff base ligand: The effect of metal on the mode of binding, Eur. J. Med. Chem. 45 (2010) 4239–4245.

[33] E.F. Healy, Quantitative determination of DNA–ligand binding using fluorescence spectroscopy, J. Chem. Educ. 84 (2007) 1304–1307.

[34] O. Stern, M. Volmer, The extinction period of fluorescence, Z. Phys. 20 (1919) 183–188.

[35] S. Bhattacharyya, A. Sarkar, S.K. Dey, G.P. Jose, A. Mukherjee, T.K. Sengupta, Copper (II) complex of methionine conjugated bis–pyrazole based ligand promotes dual pathway for DNA cleavage, Dalt. Trans. 42 (2013) 11709–11719.

[36] M.T. Carter, A.J. Bard, Voltammetric studies of the interaction of tris (1, 10–phenanthroline) cobalt (III) with DNA, J. Am. Chem. Soc. 109 (1987) 7528–7530.

[37] F. Arjmand, P. Tewatia, M. Aziz, R.H. Khan, Interaction studies of a novel Co (II)–based potential chemotherapeutic agent with human serum albumin (HSA) employing biophysical techniques, Med. Chem. Res. 19 (2010) 794–807.

[38] K.V.H. Prashanth, S.M. Dharmesh, K.S.J. Rao, R.N. Tharanathan, Free radical–induced chitosan depolymerized products protect calf thymus DNA from oxidative damage, Carbohydr. Res. 342 (2007) 190–195.

[39] (a) D.D. Lasic, H. Strey, M.C.A. Stuart, R. Podgornik, P.M. Frederik, The structure of DNA − liposome complexes, J. Am. Chem. Soc. 119 (1997) 832–833;
(b) J.S. Choi, D.K. Joo, C.H. Kim, K. Kim, J.S. Park, Synthesis of a barbell-like triblock copolymer, poly (L–lysine) dendrimer–block–poly (ethylene glycol)–-block–poly (L–lysine) dendrimer, and its self-assembly with plasmid DNA, J. Am. Chem. Soc. 122 (2000) 474–480;
(c) D. Matulis, I. Rouzina, V.A. Bloomfield, Thermodynamics of cationic lipid binding to DNA and DNA condensation: roles of electrostatics and hydrophobicity, J. Am. Chem. Soc. 124 (2002) 7331–7342;
(d) B.H. Zinselmeyer, S.P. Mackay, A.G. Schatzlein, I.F. Uchegbu, The lower-generation polypropylenimine dendrimers are effective gene–transfer agents, Pharm. Res. 19 (2002) 960–967;
(e) F.L. Sorgi, S. Bhattacharya, L. Huang, Protamine sulfate enhances lipid-mediated gene transfer, Gene Ther. 4 (1997) 961–968;
(f) A.L. Parker, D. Oupicky, P.R. Dash, L.W. Seymour, Methodologies for monitoring nanoparticle formation by self-assembly of DNA with poly (l-lysine), Anal. Biochem. 302 (2002) 75–80.

[40] H.Y. Khan, S. Zehra, S. Parveen, I. Yousuf, S. Tabassum, F. Arjmand, New ionic Cu (II) and Co(II) DACH-flufenamate conjugate complexes: spectroscopic characterization, single X-ray studies and cytotoxic activity on human cancer cell lines, ChemistrySelect. (2018), https://doi.org/10.1002/slct.201802698.

[41] R. Singh, D. Pantarotto, D. McCarthy, O. Chaloin, J. Hoebeke, C.D. Partidos, J.-P. Briand, M. Prato, A. Bianco, K. Kostarelos, Binding and condensation of plasmid DNA onto functionalized carbon nanotubes: toward the construction of nanotube–based gene delivery vectors, J. Am. Chem. Soc. 127 (2005) 4388–4396.

[42] X. Liu, H. Diao, N. Nishi, Applied chemistry of natural DNA, Chem. Soc. Rev. 37 (2008) 2745–2757.

[43] J. Zheng, Z. Li, A. Wu, H. Zhou, H. Bai, Y. Song, The structural transition of DNA–Tris (1, 10–phenanthroline) cobalt (III) complexes in ethanol–water solution, Biochem. Biophys. Res. Commun. 299 (2002) 910–915.

[44] K. Fox, Drug-DNA Interact, Protocols 90 (1997) 95–106.

[45] (a) S. Parveen, S. Tabassum, F. Arjmand, Synthesis of chiral R/S-pseudopeptide-based Cu (II) & Zn (II) complexes for use in targeted delivery for antitumor therapy: enantiomeric discrimination with CT-DNA and pBR322 DNA hydrolytic cleavage mechanism, RSC Adv. 7 (2017) 6587–6597;
(b) S.D. Kettenmann, F.R. Louka, E. Marine, R.C. Fischer, F.A. Mautner, N. Kulak, S.S. Massoud, Efficient Artificial Nucleases for Mediating DNA Cleavage Based on Tuning the Steric Effect in the Pyridyl Derivatives of Tripod Tetraamine-Cobalt (II) Complexes, Eur. J. Inorg. Chem. 2018 (2018) 2322–2338.

[46] C. Liu, L. Wang, DNA hydrolytic cleavage catalyzed by synthetic multinuclear metallonucleases, Dalt. Trans. (2009) 227–239.

[47] M.E. Branum, A.K. Tipton, S. Zhu, L. Que, Double-strand hydrolysis of plasmid DNA by dicerium complexes at 37 C, J. Am. Chem. Soc. 123 (2001) 1898–1904.

[48] Z.-C. Liu, B.-D. Wang, B. Li, Q. Wang, Z.-Y. Yang, T.-R. Li, Y. Li, Crystal structures, DNA-binding and cytotoxic activities studies of Cu (II) complexes with 2-oxo-quinoline-3-carbaldehyde Schiff-bases, Eur. J. Med. Chem. 45 (2010) 5353–5361.